IET Power Electronics

Research Article

IET Journals
The Institution of Engineering and Technology

Flexible active compensation based on load conformity factors applied to non-sinusoidal and asymmetrical voltage conditions

ISSN 1755-4535
Received on 9th February 2015
Revised on 19th June 2015
Accepted on 4th July 2015
doi: 10.1049/iet-pel.2015.0086
www.ietdl.org

Danilo Iglesias Brandao[1] ✉, *Helmo Kelis Morales Paredes*[2], *Alessandro Costabeber*[3], *Fernando Pinhabel Marafão*[2]

[1]*Department of Systems and Energy, University of Campinas, Av. Albert Einstein 400, Campinas, Brazil*
[2]*Group of Automation and Integrated Systems, UNESP – Univ. Estadual Paulista, Av. Três de Março 511, Sorocaba, Brazil*
[3]*Department of Electrical and Electronic Engineering, University of Nottingham, NG7 2RD Nottingham, UK*
✉ *E-mail: dbrandao@dsce.fee.unicamp.br*

Abstract: This study proposes a flexible active power filter (APF) controller operating selectively to satisfy a set of desired load performance indices defined at the source side. The definition of such indices, and of the corresponding current references, is based on the orthogonal instantaneous current decomposition and conformity factors provided by the conservative power theory. This flexible approach can be applied to single- or three-phase APFs or other grid-tied converters, as those interfacing distributed generators in smart grids. The current controller is based on a modified hybrid P-type iterative learning controller which has shown good steady-state and dynamic performances. To validate the proposed approach, a three-phase four-wire APF connected to a non-linear and unbalanced load has been considered. Experimental results have been generated under ideal and non-ideal voltage sources, showing the effectiveness of the proposed flexible compensation scheme, even for weak grid scenarios.

1 Introduction

The research on control techniques for active power filters (APFs) applicable to smart distribution grids and microgrids under non-sinusoidal and/or asymmetrical operations is motivated by the increasing percentage of power generated from primary energy sources interfaced through power electronics converters. Distributed generation increases the availability and reliability of the power delivery, enables an increase in power capacity without infrastructural investments but reduces the stiffness of the power system. As a consequence, the equivalent voltage source seen at the point of common coupling (PCC) of a microgrid – or in general of a distribution feeder – tends to deviate from ideality, presenting harmonic content and unbalanced fundamental voltages.

From a general perspective, APFs compensating unwanted load current components have been subject of extensive studies during the past 30 years. The contributions to this literature range from type of filters [1], filter topologies [2, 3] design of passive and active elements [4, 5], controller schemes [6–8], control strategies [9–11], power theories applied to active compensation [12–14], selective and flexible compensation objectives [15–19] and non-ideal voltage operation [20, 21]; these last two are the focus of this paper. The development of an APF controller highly depends on the adopted power theory, which directly impacts on the control strategy, filter design and compensation results. In particular, time-domain methods such as the *pq*-theory [13] and the modified *pq*-theory [11] have been the most applied strategies. There are other options, such as the i_d–i_q method [22], and many others that can be found in [6, 10, 12, 23]. However, p–q and i_d–i_q control strategies are sensitive to voltage non-idealities and their results are difficult to be analysed under distorted and asymmetric voltage conditions [9, 15, 24].

On the other hand, in a smart grid scenario with pervasive use of distributed generators (DGs), the power available from primary side of renewable DGs, such as photovoltaic or wind energy sources are often lower than the power rating of their switching power interfaces (SPIs), due mainly to their intermittent characteristics. This enables the use of the SPI in other operating modes, providing ancillary services such as unwanted current compensation in smart gird scenario. In this context, a selective compensation strategy should be considered, since it allows to design the active compensator components (switches, inductors, capacitors etc.) based on a minimum amount of particular disturbing effects (harmonics, unbalances and phase-shift) [16–19] or selected harmonics [6] and also to enhance the operation of DGs, when operating close to their power/current ratings, considering that priority is always given to active power generation from the DG.

Hence, the main goal of this paper is to use the set of load conformity factors defined in [25], as a flexible approach to define the current references for shunt APFs operating on a weak grid with unbalanced and/or distorted voltages. Such factors are based on the orthogonal (decoupled) currents decomposition described by the conservative power theory (CPT) [14]. Thus, the CPT conformity factors can be defined as load performance indices and applied as in [18, 19].

Furthermore, the proposed control strategy can generate accurate current references to reach a desired set of performance indices at the PCC by using proper scaling coefficients. As these can be adjusted independently, thanks to the decoupled nature of the CPT decomposition, the reference generator is very flexible and allows selective reduction of load disturbing effects, in any percentage, to meet whichever consumer or utility criteria.

The proposed current reference generator is defined in the time-domain, differently from [16] that proposed a flexible frequency-domain methodology, by means of recursive discrete Fourier transform. As anticipated, differently from the most traditional schemes, the proposed approach guarantees a good compensation performance even under distorted and/or asymmetrical voltage conditions that are of great relevance to the smart grid scenario. This enhancement occurs because the CPT terms are average power quantities over a line period and they are related just to the *load* undesired characteristic, inherently reducing the impact of non-idealities from the voltage source. It also does not need any kind of reference-frame transformation [15, 18] as traditional p–q and d–q methods.

Experimental results are provided to evaluate the steady-state and dynamic response of the proposed compensation scheme and also to validate the feasibility and flexibility of the proposed approach.

2 Basic concepts and definitions about CPT and the load conformity factors

The CPT [14] is a time-domain-based power theory, valid for single-phase and three-phase systems, with three or four-wire circuits, independent from the purity of voltage and current waveforms, as required by other power theories, which are more sensitive to voltage distortion and asymmetry [9].

In the following description, lowercase and uppercase variables are, respectively, instantaneous and root-mean-square (RMS) values. Boldface variables refer to vector quantities (collective values) and the subscript 'm' indicates phase variables. Such theory is valid for generic poly-phase circuits under periodic operation.

2.1 Instantaneous orthogonal currents decomposition

The CPT is based on the orthogonal decomposition of instantaneous phase currents, which can be split into different components

$$i_m = i_{am}^{\mathrm{b}} + i_{rm}^{\mathrm{b}} + i_m^{\mathrm{u}} + i_{\mathrm{v}m} = i_{am}^{\mathrm{b}} + i_{\mathrm{na}m}, \tag{1}$$

such that $i_{\mathrm{a}}^{\mathrm{b}}$ is the balanced active current; $i_{\mathrm{r}}^{\mathrm{b}}$ is the balanced reactive current; i^{u} is the unbalance current; i_{v} is the void current and i_{na} is the non-active current.

The *balanced active currents* have been determined as the minimum currents needed to convey total active power ($P = \sum_{m=1}^{M} P_m$) absorbed at the PCC. They are given by

$$i_{am}^{\mathrm{b}} = \frac{\langle \boldsymbol{v},\ \boldsymbol{i}\rangle}{\|\boldsymbol{v}\|^2}\cdot v_m = \frac{P}{\boldsymbol{V}^2}\cdot v_m = G^{\mathrm{b}}\cdot v_m, \tag{2}$$

where $\langle \boldsymbol{v},\ \boldsymbol{i}\rangle$ represents internal product, which can be calculated by the result from the dot product of voltage ($\boldsymbol{v}$) and current ($\boldsymbol{i}$) vectors through a moving average filter; $\|\boldsymbol{v}\| = \sqrt{V_a{}^2 + V_b{}^2 + V_c{}^2} = \boldsymbol{V}$ is the collective RMS value (Euclidean norm) of the voltages and G^{b} is the *equivalent balanced conductance*.

Similarly, the *balanced reactive currents* have been defined as the minimum currents needed to convey total reactive energy ($W = \sum_{m=1}^{M} W_m$) drained at the PCC. They are given by

$$i_{rm}^{\mathrm{b}} = \frac{\langle \hat{\boldsymbol{v}},\ \boldsymbol{i}\rangle}{\|\hat{\boldsymbol{v}}\|^2}\cdot \hat{v}_m = \frac{W}{\hat{\boldsymbol{V}}^2}\cdot \hat{v}_m = B^{\mathrm{b}}\cdot \hat{v}_m, \tag{3}$$

where $\hat{\boldsymbol{v}}_m$ is the phase voltage integral without average value (named *unbiased time integral*) and B^{b} is the *equivalent balanced reactivity*.

The balanced active and reactive currents always have the same waveforms of the phase voltages ($\boldsymbol{v}_m$) and the phase voltage integrals ($\hat{\boldsymbol{v}}_m$), respectively. Note that the 'balanced' term is related to load symmetry and not to current symmetry.

In a case of balanced load, the PCC only absorbs balanced active and reactive currents; otherwise it also drains *unbalance currents*, which have been defined as

$$i_m^{\mathrm{u}} = \left(G_m - G^{\mathrm{b}}\right)\cdot v_m + \left(B_m - B^{\mathrm{b}}\right)\cdot \hat{v}_m. \tag{4}$$

$$G_m = \frac{P_m}{\boldsymbol{V}_m^2};\quad G^{\mathrm{b}} = \frac{P}{\boldsymbol{V}^2}\quad \text{and}\quad B_m = \frac{W_m}{\hat{\boldsymbol{V}}_m^2};\quad B^{\mathrm{b}} = \frac{W}{\hat{\boldsymbol{V}}^2}, \tag{5}$$

such that G_m and B_m are the *phase equivalent conductance* and *reactivity*. Note that if the load is balanced the phase equivalent conductance is equal to the equivalent balanced conductance ($G_m = G^{\mathrm{b}}$). Similarly, the reactivity parameters are equal ($B_m = B^{\mathrm{b}}$).

The *void currents* are defined as the remaining phase currents. They do not convey active power or reactive energy and represent all the load non-linearity currents (harmonics). However, they cause power loss and/or electromagnetic interference in the utility lines

$$i_{\mathrm{v}m} = i_m - i_{am}^{\mathrm{b}} - i_{rm}^{\mathrm{b}} - i_m^{\mathrm{u}}. \tag{6}$$

All the previous current components are orthogonal to each other. Thus, the collective RMS current can be calculated by

$$\boldsymbol{I}^2 = \boldsymbol{I}_{\mathrm{a}}^{\mathrm{b}2} + \boldsymbol{I}_{\mathrm{r}}^{\mathrm{b}2} + \boldsymbol{I}^{\mathrm{u}2} + \boldsymbol{I}_{\mathrm{v}}^2 = \boldsymbol{I}_{\mathrm{a}}^{\mathrm{b}2} + \boldsymbol{I}_{\mathrm{na}}^2. \tag{7}$$

Accordingly, multiplying the collective RMS current and voltage, the apparent power (A) can be also split into

$$A^2 = \boldsymbol{V}^2\cdot \boldsymbol{I}^2 = P^2 + Q^2 + N^2 + D^2, \tag{8}$$

where P is the active power; Q is the reactive power; N is the unbalance power and D is the distortion power.

2.2 Load conformity factors

By means of the CPT, a set of performance indices can be defined to characterise different aspects of load operation. They are based on the orthogonal current/power decomposition and have been proposed in [25].

The general conformity factor is the *power factor* (λ), which is affected by reactive current circulation, load unbalance and current non-linearities. Unit power factor represents current waveforms proportional to voltage waveforms (as in case of balanced resistive loads)

$$\lambda = \frac{\boldsymbol{I}_{\mathrm{a}}^{\mathrm{b}}}{\sqrt{\boldsymbol{I}_{\mathrm{a}}^{\mathrm{b}2} + \boldsymbol{I}_{\mathrm{na}}^2}} = \frac{\boldsymbol{I}_{\mathrm{a}}^{\mathrm{b}}}{\boldsymbol{I}} = \frac{P}{A}. \tag{9}$$

Of course, under sinusoidal and symmetrical (or single-phase) voltage and current conditions, λ is equal to the traditional fundamental displacement factor ($\cos\phi_1$), where ϕ_1 is the phase angle between fundamental phase voltage and current. However, this relation is not correct if the grid voltages and/or currents are distorted and/or unbalanced.

The *reactivity factor* (λ_Q) has been defined as

$$\lambda_Q = \frac{\boldsymbol{I}_{\mathrm{r}}^{\mathrm{b}}}{\sqrt{\boldsymbol{I}_{\mathrm{a}}^{\mathrm{b}2} + \boldsymbol{I}_{\mathrm{r}}^{\mathrm{b}2}}} = \frac{Q}{\sqrt{P^2 + Q^2}}, \tag{10}$$

and it reveals the presence of reactive energy in linear inductors and capacitors, or even fundamental phase shifting caused by non-linear loads (e.g. thyristor rectifiers). For single-phase or balanced three-phase circuits, with sinusoidal supply voltages, λ_Q could be calculated as $\lambda_Q = \sin(\phi_1)$.

The *unbalance factor* (λ_N) has been defined as

$$\lambda_N = \frac{\boldsymbol{I}^{\mathrm{u}}}{\sqrt{\boldsymbol{I}_{\mathrm{a}}^{\mathrm{b}2} + \boldsymbol{I}_{\mathrm{r}}^{\mathrm{b}2} + \boldsymbol{I}^{\mathrm{u}2}}} = \frac{N}{\sqrt{P^2 + Q^2 + N^2}}, \tag{11}$$

which indicates possible unbalances on the *load* equivalent phase impedances (conductances and reactivities). Such factor results zero only if the load is balanced, independently of voltage symmetry or distortion.

In case of sinusoidal and symmetrical supply voltages, the unbalance factor can also be related to the traditional positive, negative and zero sequence unbalance factors, calculated by means of Fortescue's transformation on the fundamental current waveforms.

Finally, the *distortion factor* (λ_D) has been defined as

$$\lambda_D = \frac{\boldsymbol{I}_v}{\sqrt{\boldsymbol{I}_a^{b2} + \boldsymbol{I}_r^{b2} + \boldsymbol{I}^{u2} + \boldsymbol{I}_v^2}} = \frac{\boldsymbol{I}_v}{\boldsymbol{I}} = \frac{D}{A}, \tag{12}$$

which reveals the presence of load non-linearities (distortion currents). Considering single-phase or balanced three-phase loads, supplied by ideal voltages, such conformity factor may be associated to the conventional current total harmonic distortion (THD_I). $\lambda_D = 0$ means that the load is linear and G_m and B_m are constant over time.

On the basis of the previous definitions, the relationship among the initial global *power factor* and the other factors can be expressed by

$$\lambda = \sqrt{\left(1 - \lambda_Q^2\right) \cdot \left(1 - \lambda_N^2\right) \cdot \left(1 - \lambda_D^2\right)}, \tag{13}$$

which allows us to independently assess the influence of each conformity factor on the global power factor. Under ideal operation, the reactivity, unbalance and distortion factors are equal to zero, since they express the non-idealities of the power circuits, whereas the λ results unitary, since it expresses the circuit efficiency.

3 Proposed flexible compensation strategies

Following, the proposed current reference generator will be described, as well as the overall control scheme adopted for a three-phase four-wire APF.

3.1 Basic concepts behind selective compensation strategies

On the basis of the decoupled nature of the CPT current terms, the APF must generate the accurate amount of unwanted load current to vanish with the related disturbing effect at a port of interest (e.g. PCC). Then, assuming full compensation of a particular component x, the APF should simply inject/absorb the opposite unwanted load phase currents (i_{xm}), as follows:

$$i_{xm}^{*f} = -i_{xm} \tag{14}$$

such that the subscript 'x' assumes any of the previous CPT current terms (i_{rm}^b, i_m^u, i_{vm} and i_{nam}), consequently defining the selective compensation strategy.

3.2 Flexible load conformity factors compensation

The flexible conformity factor compensation is based on the idea of driving the APF to provide the minimum amount of current/power required to reach, at the PCC, a particular result. At this stage, let us assume that the current loop controller has enough bandwidth to accurately track the current references, then, we can write

$$i_{xm}^{*f} = i_{xm}^s - i_{xm}, \tag{15}$$

such that the i_{xm}^s is the source phase currents correlated to the 'x' CPT term. It is possible to rewrite the wanted source phase currents as a function of the load phase currents and a scaling coefficient, as following:

$$i_{xm}^{*s} = k_x \cdot i_{xm}, \tag{16}$$

where k_x represents the scaling coefficient associated to each CTP current component, corresponding to a specific amount of unwanted current term x that is tolerated at the PCC. Finally, replacing (16) in (15) we found

$$i_{xm}^{*f} = k_x \cdot i_{xm} - i_{xm} = i_{xm} \cdot (k_x - 1). \tag{17}$$

Note that ($k_x = 1$) means no compensation, since i_{xm}^{*f} is zero and ($k_x = 0$) means full compensation, since i_{xm}^{*f} is equal to the opposite unwanted load currents. From (16), the collective RMS value of the wanted source currents is

$$\boldsymbol{I}_x^{*s} = k_x \cdot \boldsymbol{I}_x = \sqrt{\sum_{m=0}^{M} \left(k_x \cdot I_{xm}\right)^2}. \tag{18}$$

Thus, considering all possible compensation schemes, the desired conformity factors at PCC and the scaling coefficients are calculated as follows:

$$\lambda^* = \frac{\boldsymbol{I}_a^b}{\sqrt{\boldsymbol{I}_a^{b2} + \boldsymbol{I}_{na}^{*2}}}; \tag{19}$$

$$\lambda_Q^* = \frac{\boldsymbol{I}_r^{b*}}{\sqrt{\boldsymbol{I}_a^{b2} + \boldsymbol{I}_r^{b*2}}}; \tag{20}$$

$$\lambda_N^* = \frac{\boldsymbol{I}^{u*}}{\sqrt{\boldsymbol{I}_a^{b2} + \boldsymbol{I}_r^{b2} + \boldsymbol{I}^{u*2}}}; \tag{21}$$

$$\lambda_D^* = \frac{\boldsymbol{I}_v^*}{\sqrt{\boldsymbol{I}_a^{b2} + \boldsymbol{I}_r^{b2} + \boldsymbol{I}^{u2} + \boldsymbol{I}_v^{*2}}}. \tag{22}$$

As shown in Fig. 1, the desired conformity factors are set by the *priority resolver* block, such as in [18]. It receives the measured quantities (PCC voltage, v_{PCC}; load, i_L; and filter, i_f; currents)

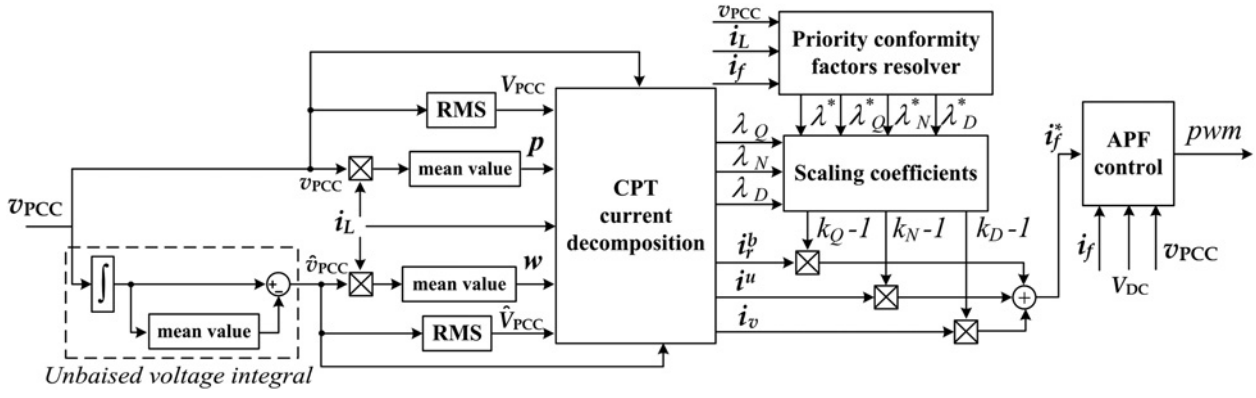

Fig. 1 *Block diagram of the flexible current reference generator*

IET Power Electron., 2016, Vol. 9, Iss. 2, pp. 356–364

and processes the references based on the filter nominal capacity and desired compensation objective.

- *Power factor compensation*

From (9) and (19) the collective RMS value of load non-active current ($\boldsymbol{I}_{\mathrm{na}}$) and wanted non-active current ($\boldsymbol{I}^{*}_{\mathrm{na}}$) can be rewritten as follows:

$$\boldsymbol{I}_{\mathrm{na}} = \frac{\boldsymbol{I}^{\mathrm{b}}_{\mathrm{a}}}{\lambda} \cdot \sqrt{1-\lambda^{2}} \quad \text{and} \quad \boldsymbol{I}^{*}_{\mathrm{na}} = \frac{\boldsymbol{I}^{\mathrm{b}}_{\mathrm{a}}}{\lambda^{*}} \cdot \sqrt{1-\lambda^{*2}}. \tag{23}$$

Then, substituting (23) in (18) we can find the non-active scaling coefficient as a function of load power factor and desired power factor (power factor reference)

$$k_{\mathrm{na}} = \frac{\lambda}{\lambda^{*}} \cdot \sqrt{\frac{1-\lambda^{*2}}{1-\lambda^{2}}}. \tag{24}$$

From (24) and (17), the flexible non-active current references are generated as

$$i^{*\mathrm{f}}_{\mathrm{na}m} = i_{\mathrm{na}m} \cdot \left(k_{\mathrm{na}} - 1\right). \tag{25}$$

When λ^{*} is unitary, the non-active scaling coefficient (24) becomes zero, making the current references equal to the opposite of non-active currents (25), leading to grid currents free of undesired load disturbing effects.

Note that the conformity factors refer to load characteristics, thus the current waveforms expected from this case should have the same waveforms of the PCC voltages.

- *Reactivity conformity factor compensation*

In a similar way, substituting (10) and (20) in (18) the reactive scaling coefficient is calculated as

$$k_{Q} = \frac{\lambda^{*}_{Q}}{\lambda_{Q}} \cdot \sqrt{\frac{1-{\lambda_{Q}}^{2}}{1-{\lambda^{*}_{Q}}^{2}}}. \tag{26}$$

It is important to recall that the compensation of the reactivity conformity factor can be performed for a three-phase system, in steady state, without energy storage components such as capacitors or reactors, as proposed in [13]. For single-phase systems the storage element is required.

- *Unbalance* conformity *factor compensation*

As before, from (11) and (21) in (18) the unbalance scaling coefficient is

$$k_{N} = \frac{\lambda^{*}_{N}}{\lambda_{N}} \cdot \sqrt{\frac{1-\lambda^{2}_{N}}{1-{\lambda^{*}_{N}}^{2}}}. \tag{27}$$

Also here, when the unbalance conformity factor reference assumes its ideal value ($\lambda^{*}_{N} = 0$), the scaling coefficient becomes zero, generating current references equal to the unbalanced load currents.

To perform this compensation strategy, even in steady state, an energy storage element is needed, because the unbalance currents can be split into unbalanced active and reactive currents [14].

- *Distortion* conformity *factor compensation*

Finally, from (12) and (22) in (18) the distortion scaling coefficient is

$$k_{\mathrm{D}} = \frac{\lambda^{*}_{\mathrm{D}}}{\lambda_{\mathrm{D}}} \cdot \sqrt{\frac{1-\lambda^{2}_{\mathrm{D}}}{1-{\lambda^{*}_{\mathrm{D}}}^{2}}}. \tag{28}$$

The effectiveness of this compensation strategy is straightly related to the bandwidth of the current control loop. Its performance is as good as the current controller capacity to track high harmonic contents.

As the void currents do not convey active power [14], the DC-link power balance is not affected by distortion compensation in steady state.

3.3 Flexible current reference generator

The ideal goal of an APF is to remove all the unwanted current components. Nevertheless, this might require significant power rating for the power converter and, consequently, higher costs. In addition, flexibility is of major importance, considering that desired requirements might change over time, especially to a smart grid scenario.

Fig. 1 shows the block diagram of the proposed current reference generator applied to a current controlled three-phase APF. Basically, it measures instantaneous voltages and currents and then it provides the CPT decomposed current terms and conformity factors. On the basis of the last three equations (26)–(28), the scaling coefficients are set and the current references for the APF are generated as

$$\boldsymbol{i}^{*}_{\mathrm{f}} = i^{*\mathrm{f}}_{m} = i^{\mathrm{b}}_{rm} \cdot \left(k_{Q} - 1\right) + i^{\mathrm{u}}_{m} \cdot \left(k_{N} - 1\right) + i_{\mathrm{v}m} \cdot \left(k_{\mathrm{D}} - 1\right). \tag{29}$$

Equation (29) is the general equation for the disturbing current compensation and indicates that the balanced active current (active power) transfer from the APF to the PCC is zero. The balanced reactive, unbalanced and harmonic current compensation can be controlled by varying the scaling coefficients. From (29), it is also found that the APF can compensate all current disturbances if $k_{Q} = k_{N} = k_{\mathrm{D}} = 0$. The filter output current, in each phase, can be calculated as

$$I^{\mathrm{est}}_{\mathrm{f}m} = \sqrt{{I^{\mathrm{b}}_{\mathrm{r}m}}^{2} \cdot \left(k_{Q} - 1\right)^{2} + {I^{\mathrm{u}}_{m}}^{2} \cdot \left(k_{N} - 1\right)^{2} + {I_{\mathrm{v}m}}^{2} \cdot \left(k_{\mathrm{D}} - 1\right)^{2}}. \tag{30}$$

Thus, the estimated output filter current (maximum capacity of the APF) should be

$$I^{\mathrm{est}}_{\mathrm{f}} = \mathrm{MAX}\left(I^{\mathrm{est}}_{\mathrm{f}a},\ I^{\mathrm{est}}_{\mathrm{f}b},\ I^{\mathrm{est}}_{\mathrm{f}c}\right). \tag{31}$$

Even if it is not addressed in this paper, under saturation condition, the scaling coefficient must adapt to deal with the filter capacity constraints and desired performance. An optimal algorithm might be applied to select a set of conformity factors for that condition, as in [18, 19]. However, even without an optimal priority resolver the proposed system is applicable, as it will always track the pre-set desired conformity factor reference, even under external perturbation.

4 APF control loop scheme

The proposed control is shown in Fig. 2. The 4-leg 2-level inverter is modulated with sine-triangle pulse-width modulation, and the fourth leg is modulated with duty cycle equal to 50%, that is, zero average voltage with respect to the centre of the DC link. This choice is due to the fact that the operating condition does not require the exploitation of the additional degree of freedom given by the neutral leg voltage. To ensure constant voltage at the DC link (V_{DC}), a proportional–integral (PI)-based controller has been used

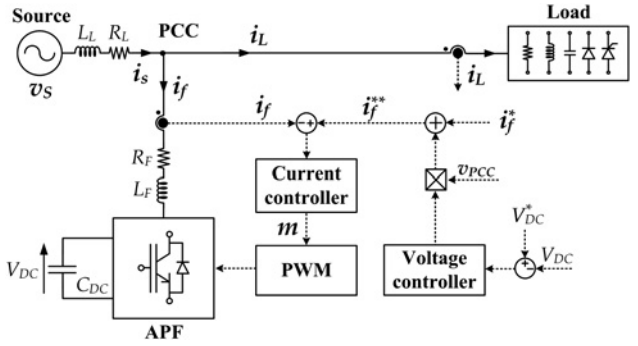

Fig. 2 *Block diagram of the APF control loop scheme*

as DC-link voltage regulator. The PI gains were designed by the classical phase margin – cross-over frequency design method and are shown in Table 1. The output of the voltage controller is multiplied by a normalised PCC voltage (v_{PCC}), to generate the active current component required to balance the converter losses, and corresponds to resistive load synthesis [10].

Then, the output of the multiplication is added to the current references (i_f^*), delivered by the flexible current reference generator (from Fig. 1). Finally, it leads to the reference of the current control loop (i_f^{**}). Thus, the APF acts as a high-power factor controlled rectifier during load transient conditions and as an active current compensator under steady state.

Observe that there is no use of any reference-frame transformations or synchronisation algorithms to generate the filter current references or to control the APF. The absence of synchronisation algorithms is valid for a certain range of frequency variation (≃0.5−1% of nominal frequency), due to the moving average filters used in CPT decompositions, tuned at the fundamental frequency. The absence of a synchronisation algorithm or reference transformation in normal operation, improves the filter performance under non-ideal voltage source.

The three-phase APF has to be able to track harmonic current references. Therefore, the proposed current controller in the *abc* frame must have large bandwidth and high gain at the relevant harmonic frequencies. This can be achieved using resonant controllers or repetitive controllers, since a PI controller would not be able to provide the same gain at high frequencies, while maintain a stable closed loop. In the implementation of the flexible active compensator, an iterative learning control (P-type ILC) structure has been used [7]. A P-type ILC controller is a different formulation of a repetitive controller, with the advantage of simplifying the design process. The dynamic response of an ILC scheme is inherently slow, due to the one fundamental period delay on which the repetitive control action relies. Even if the steady-state performance is satisfactory, this can degrade the effectiveness of the compensation during load variations. To

Table 1 Parameters of APF

APF	
Nominal apparent power = 6.5 kVA; Source line-to-line voltage = 220 V (60 Hz) Coupling inductance (L_{Fm}) = 1.5 mH Inductor resistance (R_{Fm}) = 0.1 Ω DC-link capacitor (C_{DC}) = 4.7 mF current sensor gain = 1/35 AC voltage sensor gain = 1/350 DC voltage sensor gain = 1/500 sampling frequency = 12 kHz switching frequency = 12 kHz	
Voltage loop	Current loop
K_P = 3.66; K_I = 30.18	K_P = 1.15; K_I = 1200; K_L = 0.8; m = 3; N = 200

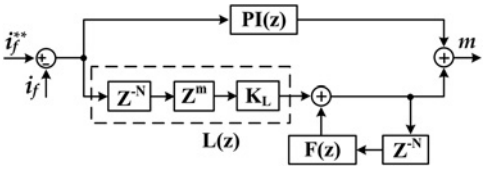

Fig. 3 *Block diagram of the PI-ILC current controller*

enhance the dynamic response, a PI-based controller is added in parallel to the ILC, as shown in Fig. 3. In a qualitative description, the PI regulator compensates for the fast part of the transients but cannot guarantee small tracking errors in steady state, whereas the ILC responds slowly but compensates for the tracking errors left by the PI.

The adopted design procedure follows the one proposed in [7]. It is based on a two-step procedure: (i) the PI regulator is designed to guarantee stability of the closed loop, neglecting the presence of the parallel ILC controller and considering the converter as the design plant. (ii) The ILC controller is designed considering as design plant of both the converter and the pre-designed PI regulator. In this way, a stable design of the overall system can be achieved. According to (i) the PI controller is first designed neglecting the ILC controller and, for this paper, the design targets were 75° of phase margin and 700 Hz of cross-over frequency. K_P and K_I in Table 1 are the PI gains resulting from this design (before discretisation). The Bode plot is shown in Fig. 4.

If the preliminary design of the PI regulator is straightforward, and can be done in the Laplace domain followed by discretisation, the design of the ILC in Fig. 3 requires a more careful design in Zeta domain. Referring to [7] and to Fig. 3, N is the total number of samples at the fundamental period of the signal in which we want

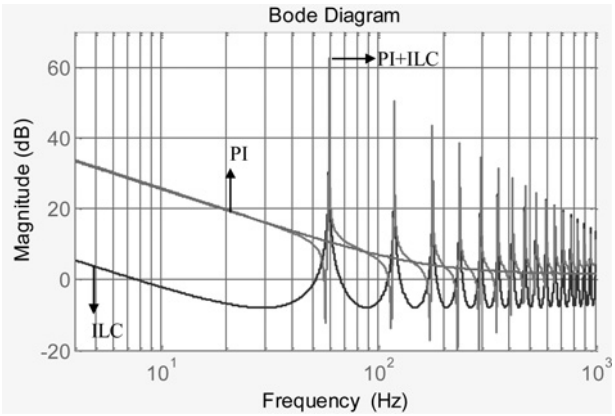

Fig. 4 *Bode plot of the designed current controller (magnitude only)*

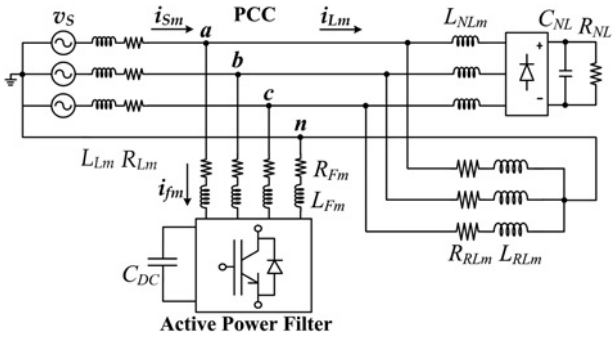

Fig. 5 *Non-linear and unbalanced three-phase four-wire circuit*

IET Power Electron., 2016, Vol. 9, Iss. 2, pp. 356–364

Table 2 Parameters of source voltages and loads

Load parameters
$R_{RLa} = 4.4\ \Omega$; $L_{RLa} = 15$ mH; $R_{RLb} = 4.1\ \Omega$; $L_{RLb} = 18$ mH; $R_{RLc} = 3.7\ \Omega$; $L_{RLc} = 30$ mH $L_{NLa} = 1$ mH; $L_{NLb} = 1$ mH; $L_{NLc} = 1$ mH; $R_{NL} = 42\ \Omega$; $C_{NL} = 2.35$ mF
Sinusoidal three-phase source (60 Hz)
$V_{Sa} = 127\angle 0°$ V; $V_{Sb} = 127\angle -120°$ V; $V_{Sc} = 127\angle 120°$ V; $L_{Lm} = 0.5$ mH; $R_{Lm} = 0.05\ \Omega$
Distorted and asymmetrical three-phase source (60 Hz)
$V_{Sa} = 122\angle 0° + 3.7\angle 3{\cdot}0° + 3.7\angle 5{\cdot}0° + 1.8\angle 7{\cdot}0°$V; $V_{Sb} = 127\angle -120° + 3.8\angle 3{\cdot}(-120°) + 3.8\angle 5{\cdot}(-120°) + 1.9\angle 7{\cdot}(-120°)$V; $V_{Sc} = 115\angle 120° + 3.4\angle 3{\cdot}(120°) + 3.4\angle 5{\cdot}(120°) + 1.7\angle 7{\cdot}(120°)$V

the repetitive action. $L(z)$ and $F(z)$ have been called in [7] 'learning factor' and 'forgetting factor', and can be generic digital filters. Note that if $L(z) = F(z) = 1$ the ILC becomes an ideal repetitive controller. The addition of $L(z)$ and $F(z)$ provides the degrees of freedom required to ensure stability of the closed-loop system. In this implementation, $L(z)$ is composed by a gain K_L and a phase-shift $m-N$. K_L changes the total gain of the controller, whereas $m-N$ is a phase gain (a delay of $m-N$ corresponds to an advance of m). To limit the degrees of freedom in the design, $F(z)$ has been set as a moving average filter over two samples, with the goal of reducing the amplitude of the repetitive peaks. In conclusion, the design of the ILC controller depends on the choice of m and K_L. To maximise the gain, K_L has been set to 0.8, and m has been derived by simulation to guarantee that the Nyquist diagram of the loop gain (including converter, PI and ILC) remains within the unit circle, guaranteeing stability. Note that the design procedure is iterative, and the choice of specific constraints (as $F(z)$ and K_L in this design) not always leads to a stable solution and might require the exploitation of all the degrees of freedom.

5 Experimental results

5.1 Setup description

The power circuit applied to the experimental validation is a non-linear and unbalanced three-phase four-wire network, as in Fig. 5. The active filter prototype was based on a three-phase four-leg voltage source converter using insulated gate bipolar transistors (IGBTs – SKM 100GB128D, driven by an SKPC 22/2 – both from Semikron). The digital controllers were implemented in a fixed-point digital signal processor (TMSF2812) from Texas Instruments. Details of the source voltages (v_s) and loads are shown in Table 2. The APF and its control parameters are in Table 1.

5.2 Operation under sinusoidal voltage source

To evaluate the proposed flexible strategies and the designed voltage and current controllers, the system of Fig. 5 has been implemented and tested under sinusoidal voltage source. The results are depicted in Fig. 6.

Fig. 6*a*. shows the instantaneous three-phase PCC voltages and load currents, including neutral wire current, without compensation ($k_Q = k_N = k_D = 1$). Note that the PCC voltages are slightly distorted and asymmetric due to the effect of the non-linear and unbalance currents flowing through the line impedances. The RMS and THD values of the load phase currents are: 20.9 A, 10.98% (phase *a*); 17.4 A, 13.33% (phase *b*); and 16.1 A, 14.73% (phase *c*). See Table 3 for more details regarding to the RMS and THD voltage and current values. Moreover, the load unbalance effect can be observed by the neutral current.

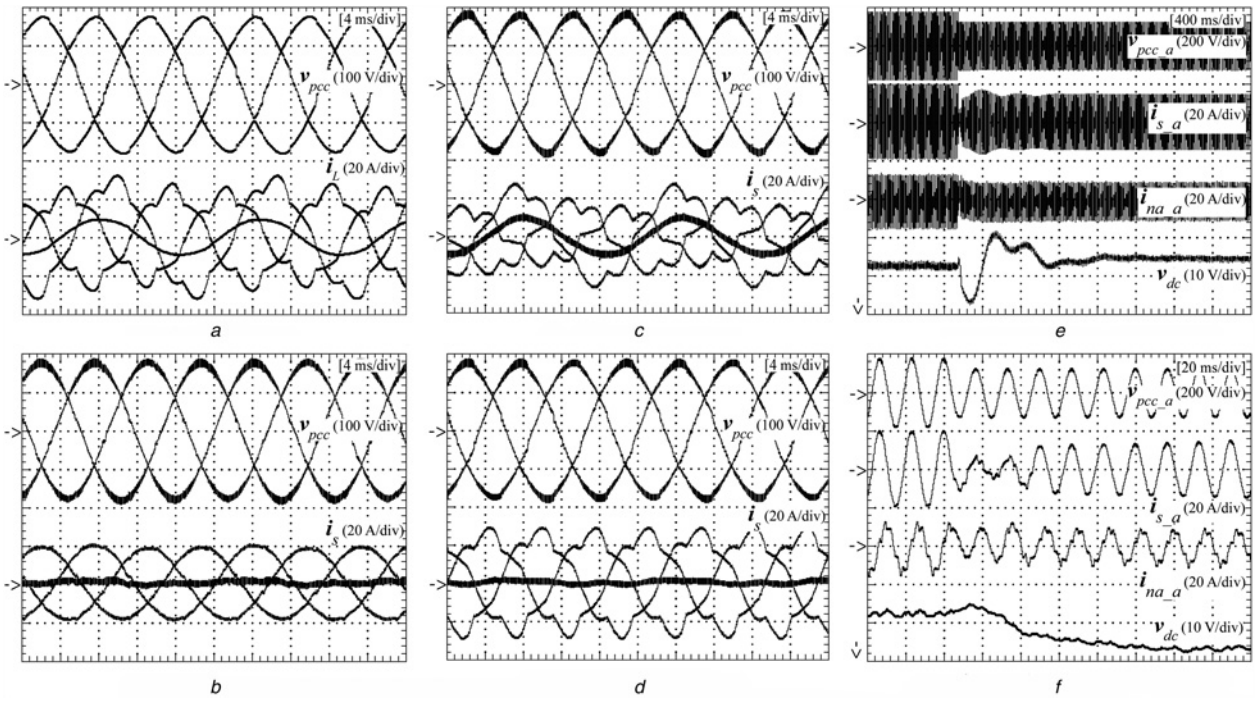

Fig. 6 *Selective load current compensation under sinusoidal voltage source operation*

a Load ($k_Q = k_N = k_D = 1$)
b i_{na} ($k_Q = k_N = k_D = 0$)
c i_r^b ($k_Q = 0$ and $k_N = k_D = 1$)
d i^u ($k_N = 0$ and $k_Q = k_D = 1$)
e Step-down voltage variation
f Step-down voltage variation (zoom)

Table 3 PCC voltages, currents and power and filter currents of selective compensation under sinusoidal voltage source operation

Parameters	Load	i_{na}	i_r^b	i^u	i_v
***A*, kVA**	6.71	5.02	5.21	6.67	6.71
***P*, kW**	4.46	5.01	4.96	4.69	4.69
***Q*, kVAr**	4.80	**0.03** [1]	**0.01**	4.65	4.64
***N*, kVA**	1.16	**0.1**	1.25	**0.08**	1.16
***D*, kVA**	0.92	**0.36**	0.95	0.9	**0.38**
V_a, V	122.3	124.8	124.6	**122.5**	122.3
THD, %	2.29	0.92	2.14	2.24	**0.81**
V_b, V	121.9	124.5	124.3	**122.3**	121.8
THD, %	2.27	0.87	2.20	2.18	**0.84**
V_c, V	123.4	125.4	126	**123.3**	123.7
THD, %	2.26	0.9	2.25	2.22	**0.8**
I_{sa}, A	20.88	**13.74**	17.81	18.39	20.98
THD, %	10.98	**3.13**	13.6	12.41	2.08
I_{sb}, A	17.43	**13.21**	12.77	17.97	17.34
THD, %	13.33	**2.2**	19.27	12.87	1.8
I_{sc}, A	16.12	**13.24**	10.01	18	15.97
THD, %	14.73	**1.82**	25.06	12.79	1.76
I_{fa}, A	–	13.3	13.1	3.2	2.2
I_{fb}, A	–	13.7	13.2	1.2	3.3
I_{fc}, A	–	14.3	13	4.1	2.7

[1] Notes: Data of particular interest has been bolded in Tables 3–10

In Fig. 6*b* the scaling coefficients are set to zero ($k_Q = k_N = k_D = 0$), which means full power factor compensation. This strategy leads to ideal source currents: waveforms are practically sinusoidal (see THD in Table 3), in phase with PCC voltages and free of unbalanced components, even the neutral wire current is close to zero. However, this full compensation needs a significant amount of current/power rating of the inverter, increasing its cost. See Table 3 for a quantitative analysis of RMS current values in each compensation strategy.

Figs. 6*c* and *d* show the reactivity ($k_Q = 0$ and $k_N = k_D = 1$) and unbalance ($k_N = 0$ and $k_Q = k_D = 1$) conformity factor compensations, respectively. In the first, only the reactive power is compensated, whereas in the second only the unbalance power is minimised.

Table 4 Flexible reactivity conformity factor compensation (λ_Q^* and $k_N = k_D = 0$)

λ_Q^*	**0.00**	**0.30**	**0.44**	**0.52**
λ	0.960	0.918	0.867	0.826
λ_Q	**0.000**	**0.301**	**0.439**	**0.523**
λ_N	0.215	0.205	0.196	0.186
λ_D	0.185	0.182	0.176	0.167

Table 5 Flexible unbalance conformity factor compensation (λ_N^* and $k_Q = k_D = 0$)

λ_N^*	**0.00**	**0.05**	**0.10**	**0.12**
λ	0.701	0.709	0.689	0.698
λ_Q	0.706	0.697	0.715	0.705
λ_N	**0.013**	**0.053**	**0.096**	**0.111**
λ_D	0.141	0.139	0.138	0.141

To evaluate the dynamic behaviour of the DC-link voltage controller, a 30% step down on the PCC voltage was applied to evaluate the system response under external disturbances. The results are shown in Figs. 6*e* and 7*f*. The corresponding DC voltage varies about ±10 V and follows the load time constant. From Fig. 6*f*, it is possible to observe that the source current becomes sinusoidal after three cycles.

Moreover, in order to evaluate the flexible selective compensation capability and its practical feasibility, we decided to set two scaling coefficients and then vary the third one. Tables 4–6 show the following configurations: (λ_Q^* and $k_N = k_D = 0$); (λ_N^* and $k_Q = k_D = 0$); and (λ_D^* and $k_Q = k_N = 0$).

Finally, in Table 7 it is shown a result where all the load conformity factors have been selectively driven by the set of

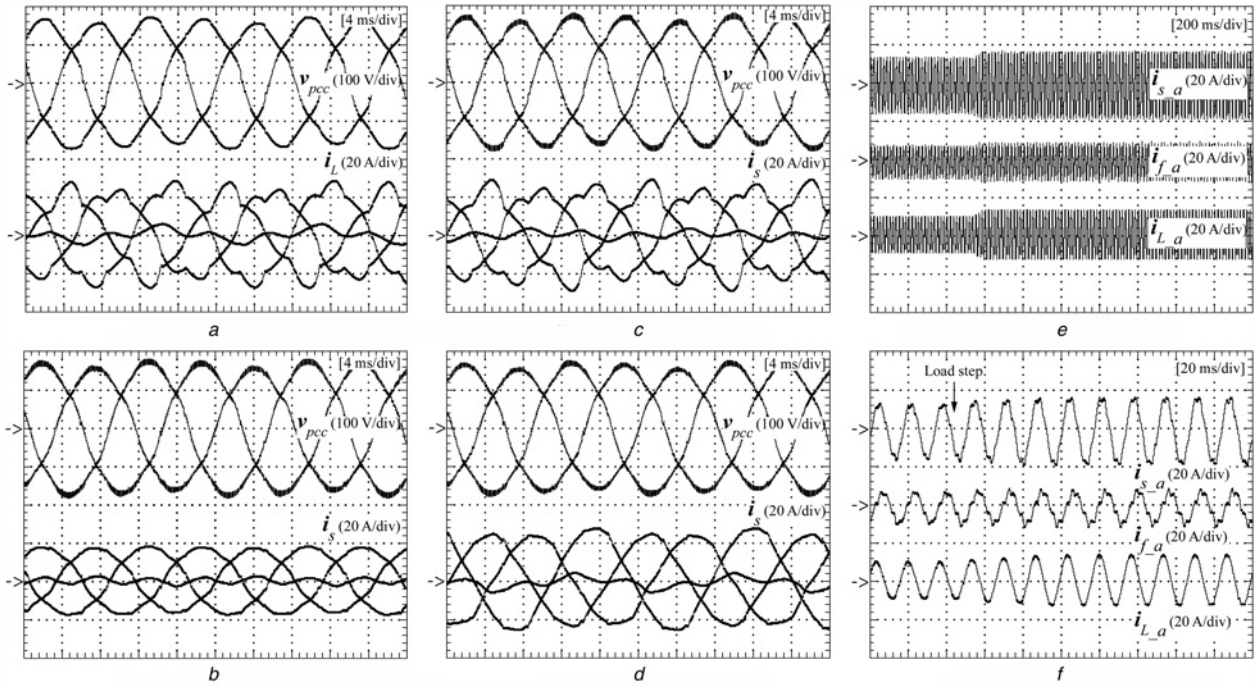

Fig. 7 *Selective load current compensation under distorted and asymmetrical voltage source operation and load step variation*

a Load ($k_Q = k_N = k_D = 1$)
b i_{na} ($k_Q = k_N = k_D = 0$)
c i^u ($k_N = 0$ and $k_Q = k_D = 1$)
d i_v ($k_D = 0$ and $k_Q = k_N = 1$)
e Step-up load variation
f Step-up load variation (zoom)

Table 6 Flexible distortion conformity factor compensation (λ_D^* and $k_Q = k_N = 0$)

λ_D^*	**0.00**	**0.08**	**0.10**	**0.12**
λ	0.693	0.686	0.694	0.682
λ_Q	0.712	0.717	0.708	0.718
λ_N	0.152	0.154	0.154	0.154
λ_D	**0.061**	**0.088**	**0.106**	**0.126**

references (λ_Q^*, λ_N^*, λ_D^*). From these set of conformity factors and (13), it is possible to calculate the expected power factor.

5.3 Operation under distorted and asymmetrical voltage source

To evaluate the selective compensation under non-ideal voltage conditions, the load was supplied by distorted and asymmetrical voltages, as shown in Table 2. Fig. 7 and Table 8 report the corresponding results.

Fig. 7*a* shows the instantaneous three-phase PCC voltages and load currents, including neutral wire current, without compensation ($k_Q = k_N = k_D = 1$). In this case, a portion of neutral wire current is caused by the unbalanced load and other portion is caused by the distorted and asymmetrical voltages.

Fig. 7*b* shows the full power factor compensation ($k_Q = k_N = k_D = 0$) under non-ideal voltage source operation. As expected, the source current waveforms assume the same waveforms of the PCC voltages, and the neutral wire current is reduced to the contribution from the grid voltage non-ideality.

Fig. 7*c* shows the unbalance ($k_N = 0$ and $k_Q = k_D = 1$) conformity factor compensation under distorted and asymmetrical voltages. Note that the unbalance power is minimised; however, the neutral current is not eliminated due to the asymmetry existing in the voltages.

Following, Fig. 7*d* shows the distortion ($k_D = 0$ and $k_Q = k_N = 1$) factor compensation under these non-ideal voltages. In this case, one can note that even reducing the distortion power (void currents), the resulting currents are still distorted due to the influence of the distorted source voltages, which affects the other three current components (active, reactive and unbalanced). See Table 8 for a detailed analysis.

Table 7 Flexible current reference generator (λ_Q^*, λ_N^*, λ_D^*)

$\lambda_Q^* = 0.2$	$\lambda_N^* = 0.1$	$\lambda_D^* = 0.08$	$\lambda^* = 0.972$
0.2	0.115	0.084	0.97

Table 8 PCC voltages, currents and power and filter currents for selective compensation under distorted and asymmetrical voltage source

Parameters	Load	i_{na}	i_r^b	i^u	i_v
***V*, A**	202.5	206.6	206.4	202.7	202.5
***I*, A**	29.5	21.7	22	29.6	29.7
***A*, kVA**	6.03	4.48	4.64	6.03	6.06
***P*, kW**	3.95	4.48	4.46	4.16	4.23
***Q*, kVAr**	4.4	**0.01**	**0.01**	4.27	4.24
***N*, kVA**	0.86	**0.07**	0.92	**0.07**	0.89
***D*, kVA**	0.87	**0.21**	0.92	0.9	**0.26**
V_a, V	110.9	112.7	112.9	110.9	111
THD, %	5.76	4.52	5.77	5.91	4.85
V_b, V	122.3	124.3	124.9	122.2	122.2
THD, %	6.13	4.92	6.21	6.37	5.11
V_c, V	117.5	120.4	119.9	118	117.4
THD, %	6.76	4.71	6.6	6.34	5.42
I_{sa}, A	16.3	12.1	14.6	16.5	16.4
THD, %	13.07	5.54	16.36	13.77	5.05
I_{sb}, A	18.7	12.9	13.6	17.6	18.8
THD, %	10.08	5.95	15.77	10.54	4.14
I_{sc}, A	16.5	12.6	10.4	17.4	16.3
THD, %	15.63	6.04	27.69	16.25	4.41

Table 9 Flexible power factor compensation

λ^*	**0.98**	**0.95**	**0.92**	**0.9**
λ	**0.981**	**0.958**	**0.929**	**0.916**
λ_Q	0.179	0.27	0.353	0.383
λ_N	0.048	0.069	0.083	0.09
λ_D	0.059	0.074	0.087	0.094

Table 10 Flexible unbalance conformity factor compensation (λ_N^* and $k_Q = k_D = 0$)

λ_N^*	**0.05**	**0.08**	**0.1**	**0.12**
λ	0.68	0.684	0.668	0.689
λ_Q	0.725	0.72	0.735	0.713
λ_N	**0.056**	**0.085**	**0.104**	**0.122**
λ_D	0.146	0.144	0.14	0.144

Finally, to validate the selective compensation and its feasibility under non-ideal conditions, we have applied the global power factor compensation (λ^*) using (25) and the unbalance conformity factor compensation (λ_N^* and $k_Q = k_D = 0$). These results are reported in Tables 9 and 10, where the effectiveness of these strategies has been confirmed even under operation with non-sinusoidal mains.

5.4 Discussion of computational complexity

The CPT current decompositions and load conformity factors calculation require high computational efforts [26]. However, for most applications they do not need to be processed in real time. Thus, the CPT calculation could run into a low-frequency loop or in case of a three-phase APF, the phase equivalent conductance and reactivity [G_m and $B_m$from (2) to (5)] of each phase could be updated within a period of fundamental cycle. Thus, each phase quantity would be processed into a period of three fundamental cycles.

This strategy may be used when facing computational limitations and it may cause a delayed transient response resulting under or over compensation until the next update. However, such strategy was applied to generate all the paper's results, and as it was observed, it led to an acceptable dynamic performance taking only few line periods to convergence, as reported in Figs. 7*e* and *f*.

5.5 Discussion about the dynamic response under load steps

To evaluate the reference generator and designed current controller under load variations, the DC link was imposed by a DC power source, aiming to observe the dynamic response of the currents without the effect of the link voltage regulator. A step up of 20% of the nominal load power was applied, and the result is shown in Figs. 7*e* and *f*.

The transient lasts few line periods and it is not related to the current controller dynamic, which is faster (refers to Section 4). Indeed, as mentioned previously, the dynamics is dominated by the current reference generator. The applied moving average filters inherently have one cycle response. Then, the observed response is due to the computational strategy used to update the G_m and B_m, as explained in Section 5.4.

6 Conclusions

This paper presented a three-phase APF controlled in stationary (*abc*) coordinates using a flexible current reference generator, which is based on orthogonal instantaneous current decomposition from CPT and a defined set of conformity factors related to specific load disturbing effects. The conformity factors can be set to any references between their ideal value (full compensation) and the non-compensation case, through the definition of

appropriate scaling coefficients, thus offering a flexible tool when full compensation is not possible. The scaling coefficients allow the system to reach accurate desired conformity factors at the grid side (PCC).

The flexible current reference generator might be applied to single-phase or three-phase APF as well as to other grid-tied converters, as those for renewable DGs. The provided current references for flexible compensation have been tracked by modified hybrid P-type iterative learning current controller, which has shown good steady-state and dynamic performances even to high-frequency harmonics. The control scheme does not use reference-frame transformation or synchronisation algorithm, which simplifies its understanding and improves its operation under non-ideal voltage source. The proposed solution has been validated through theoretical and experimental results, under ideal and non-ideal voltage source operations.

7 Acknowledgments

The authors are grateful to FAPESP (2012/24309-8, 2012/14014-0 and 2013/08545-6), CNPq (proc. 487471/2012-1) for the support provided to this research.

8 References

1 Singh, B., Al-Haddad, K., Chandra, A.: 'A review of active filters for power quality improvement', *IEEE Trans. Ind. Electron.*, 1999, **46**, (6), pp. 960–971
2 Peng, F.Z.: 'Harmonic sources and filtering approaches', *IEEE Ind. Appl. Mag.*, 2001, **7**, (4), pp. 18–25
3 Zhang, L., Waite, M.J., Chong, B.: 'Three-phase four-leg flying-capacitor multi level inverter-based active power filter for unbalanced current operation', *IET Power Electron.*, 2013, **6**, (1), pp. 153–163
4 Thomas, T., Haddad, K., Joos, G., *et al.*: 'Design and performance of active power filters', *IEEE Ind. Appl. Mag.*, 1998, **4**, (5), pp. 38–46
5 Khadem, S.K., Basu, M., Conlon, M.F.: 'Harmonic power compensation capacity of shunt active power filter and its relationship with design parameters', *IET Power Electron.*, 2014, **7**, (2), pp. 418–430
6 Mattavelli, P., Marafão, F.P.: 'Repetitive-based control for selective harmonic compensation in active power filters', *IEEE Trans. Ind. Electron.*, 2004, **51**, (5), pp. 1018–1024
7 Liu, J., Zanchetta, P., Degano, M., *et al.*: 'Control design and implementation for high performance shunt active filters in aircraft power grids', *IEEE Trans. Ind. Electron.*, 2012, **59**, (9), pp. 3604–3613
8 Chauhan, S.K., Shah, M.C., Tiwari, R.R., *et al.*: 'Analysis, design and digital implementation of a shunt active power filter with different schemes of reference current generation', *IET Power Electron.*, 2014, **7**, (3), pp. 627–639
9 Montero, M.M., Cadaval, E.R., González, F.B.: 'Comparison of control strategies for shunt active power filters in three-phase four wire system', *IEEE Trans. Power Electron.*, 2007, **22**, (1), pp. 229–236
10 Nunez-Zuniga, T.E., Pomilio, J.A.: 'Shunt active power filter synthesizing resistive loads', *IEEE Trans. Power Electron.*, 2002, **17**, (2), pp. 273–278
11 Herrera, S.R., Salmerón, P., Kim, H.: 'Instantaneous reactive power theory applied to active power filter compensation: different approaches, assessment, and experimental results', *IEEE Trans. Ind. Electron.*, 2008, **55**, (1), pp. 184–196
12 Depenbrock, M., Staudt, V.: 'The FBD-method as tool for compensating total non-active currents'. Proc. Int. Conf. Harmonics and Quality of Power, Athens, Greece, October 1998, pp. 320–324
13 Akagi, H., Kanazawa, Y., Nabae, A.: 'Instantaneous reactive power compensators comprising switching devices without energy storage components', *IEEE Trans. Ind. Appl.*, 1984, **20**, (3), pp. 625–630
14 Tenti, P., Paredes, H.K.M., Mattavelli, P.: 'Conservative power theory, a framework to approach control and accountability issues in smart microgrids', *IEEE Trans. Power Electron.*, 2011, **26**, (3), pp. 664–673
15 Campanhol, L.B.G., da Silva, S.A.O., Goedtel, A.: 'Application of shunt active power filter for harmonic reduction and reactive power compensation in three-phase four-wire systems', *IET Power Electron.*, 2014, **7**, (11), pp. 2825–2836
16 Ginn, H., Chen, G.: 'Flexible active compensator control for variable compensation objectives', *IEEE Trans. Power Electron.*, 2008, **23**, (6), pp. 2931–2941
17 Ahmadi, D., Wang, J.: 'Online selective harmonic compensation and power generation with distributed energy resources', *IEEE Trans. Power Electron.*, 2014, **29**, (7), pp. 3738–3747
18 Singh, B., Verma, V.: 'Selective compensation of power quality problems through active power filter by current decomposition', *IEEE Trans. Power Deliv.*, 2008, **23**, (2), pp. 792–799
19 Chang, G.W.: 'A new approach for optimal shunt active power filter control considering alternative performance indices', *IEEE Trans. Power Deliv.*, 2006, **21**, (1), pp. 406–413
20 Biricik, S., Redif, S., Ozerdem, O.C., *et al.*: 'Real-time control of shunt active power filter under distorted grid voltage and unbalanced load condition using self-tuning filter', *IET Power Electron.*, 2014, **7**, (7), pp. 1895–1905
21 Rahmani, B., Bina, M.T.: 'Reciprocal effects of the distorted wind turbine source and the shunt active power filter: full compensation of unbalance and harmonics under 'capacitive non-linear load' condition', *IET Power Electron.*, 2013, **6**, (8), pp. 1668–1682
22 Verdelho, P., Marques, G.D.: 'An active power filter and unbalanced current compensator', *IEEE Trans. Ind. Electron.*, 1997, **44**, (3), pp. 321–328
23 Chen, Z., Wang, Z., Chen, M.: 'Four hundred hertz shunt active power filter for aircraft power grids', *IET Power Electron.*, 2014, **7**, (2), pp. 316–324
24 Ginn, H.L.: 'Comparison of applicability of power theories to switching compensator control', *Prz. Elektrotech.*, 2013, **6**, pp. 1–10
25 Marafão, F.P., Souza, W.A., Liberado, E.V., *et al.*: 'Load analyser using conservative power theory', *Prz. Elektrotech.*, 2013, **12**, pp. 1–6
26 Mortezaei, A., Lute, C., Simões, M.G., *et al.*: 'PQ, DQ and CPT control methods for shunt active compensators – a comparative study'. Proc. IEEE Energy Conversion Congress and Exposition, Pittsburgh, USA, September 2014, pp. 2994–3001